J. Fluid Mech. (1995), *vol.* 299, *pp.* 241–265

Interfacial instabilities in plane Poiseuille flow of two stratified viscoelastic fluids with heat transfer. Part 1. Evolution equation and stability analysis

By SANG W. JOO

Department of Mechanical Engineering, Wayne State University, Detroit, MI 48282, USA

(Received 13 April 1994 and in revised form 5 January 1995)

An evolution equation is derived that describes the nonlinear development of the interface between two viscoelastic fluids flowing, under the action of imposed pressure gradient and gravity, in a vertical channel. The channel walls are kept at different temperatures, resulting in heat transfer across the layers. The equation, based on the lubrication approximation, models the effects of stratifications in density, viscosity, elasticity, shear thinning, and thermal conductivity. It also describes the capillary and thermocapillary effects, as well as the sensitivity of viscosities to temperature. Linear-stability analysis is performed based on the evolution equation to understand the competing effects of viscous, elastic, and Marangoni instabilities. Particular attention is paid to the active control of the interfacial instabilities through the thermocapillarity.

1. Introduction

The flow of multilayer non-Newtonian fluids occurs in many modern engineering processes, including the coextrusion of polymer melts. One of the important issues in this multiphase flow is the stability of the interface between different fluids. An initially flat undisturbed interface can become corrugated as the fluids flow downstream. For viscoelastic fluids, the main mechanisms for this interfacial instability are due to the velocity-gradient and normal-stress-difference mismatch at the interface, caused by the viscosity stratification and fluid elasticity, respectively. Since the interface shape can greatly influence the mechanical and optical properties of the product, an efficient control of the instability is required.

In most applications, it may be necessary to maintain the interface free of any type of corrugations, while, in other cases, it may be desirable to obtain a wavy interface with a particular wavenumber or amplitude. An efficient stability control requires precise knowledge of the linear stability of the system and the nonlinear flow developments of the unstable interfaces. In this study, we examine the effect of thermocapillarity on the viscous and elastic instabilities as a method of active stability control. Imposing a temperature difference between channel walls is relatively easy to implement in practice. The study of competing instabilities is also of great academic interest.

The instability due to the viscosity stratification in plane Poiseuille flows has been studied by Yih (1967), who performed a linear-stability analysis for two stratified

Newtonian fluids. He applied long-wave asymptotics to the Orr–Sommerfeld-type disturbance equation, and showed a purely viscous (no density stratification or thickness difference) long-wave instability. Hooper & Grimshaw (1985) studied nonlinear interface developments by deriving the Kuramoto–Sivashinsky equation and performing a weakly nonlinear analysis. They showed that a finite-ampitude steady state can be reached through nonlinear saturation. Yiantsios & Higgins (1988) later generalized Yih's analysis to account for the differences in density and layer thickness. They solved the full linear disturbance equation numerically, so that the analysis is also extended to arbitrary wavenumbers. In addition to the interfacial mode, reported by Yih, a new shear-mode instability is found. The shear mode corresponds to short-wave disturbances of Tollmien–Schlichting type, and occurs only when the Reynolds number is sufficiently large. Charru & Fabre (1994) studied the long waves at the interface in plane Couette–Poiseuille flow by deriving an interface evolution equation. Tilley, Davis & Bankoff (1994*a*) more recently reported a weakly-nonlinear analysis of the interfacial mode. They derived a strongly nonlinear evolution equation for the interface deformation by applying a long-wave approximation to the original fully coupled system. They then considered small-amplitude disturbances to obtain weakly nonlinear evolution equations of the Kuramoto–Sivashinsky type. Their nonlinear flow behaviours include the disappearance of the symmetry-breaking bifurcations due to the cubic nonlinearity introduced and a hysteresis loop that reveals the transition between smaller- and larger-amplitude travelling waves, which can be related to the phenomena of flooding.

The instability due to the fluid elasticity in stratified flows has been studied by numerous investigators, as reviewed in the works by Su & Khomami (1992*a*) and Larson (1992). Li (1969) extended Yih's (1967) Newtonian analysis to include the effect of the thickness and elasticity ratios. He showed that the purely viscous instability (interfacial mode) occurs when the less-viscous layer occupies sufficiently more space than the more-viscous one. However, he, and a few others later, incorrectly reported that the elastic instability occurs only in conjunction with the viscous instability. The correct elastic instability has been analysed more recently by Renardy (1988), Chen (1991), Su & Khomami (1992*a*,*b*). Their linear-stability analyses show that, even in the absence of the viscosity stratification, a pure elastic instability can occur, if the less-elastic layer has larger thickness. A weakly nonlinear analysis was recently performed by Renardy & Renardy (1993) to investigate the sideband instabilities following the onset of travelling interfacial waves in a stratified Couette–Poiseuille flow. They suggest that, owing to the sideband instability, the flow may be eventually dominated by the long-wave interfacial mode.

The analysis of non-isothermal stratified flows has been attempted by a number of investigators, as cited in the works of Sornberger, Vergnes & Agassant (1986) and Nordberg & Winter (1990). However, the interfacial instability in such systems is still poorly understood. The temperature control of coextruded polymer fluids is often used in practice, in order to match the viscosity at the interface and consequently suppress the instability. As noted by Nordberg & Winter (1990), this common practice of matching the zero-shear-rate viscosity is too simplistic to be effective. One must understand the interaction of the heat-transfer effects with the existing viscous and elastic instabilities.

In the present study, we examine the effect of thermocapillarity, and investigate the active stability control of stratified flows through the wall-temperature adjustment. We extend the work of Tilley *et al.* (1994*a*) to derive a strongly nonlinear evolution equation that models the effects of stratification in density, viscosity, elasticity, shear

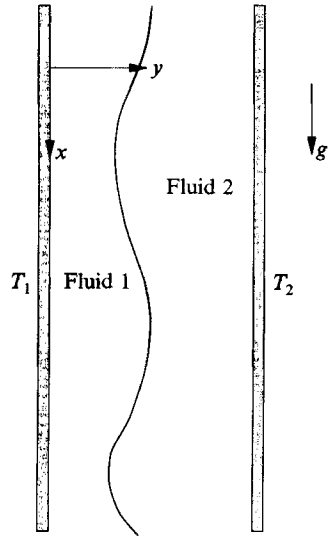

FIGURE 1. Two-layer flow configuration.

thinning, thermal thinning, and thermal conductivity. Three distinct instability mechanisms are built in, which include the thermocapillary instability of the interfacial mode. The other mode of thermocapillary instability, with much shorter characteristic wavelength, occurs in layers much thicker than those considered here, and does not generate significant interfacial deformations (see Goussis & Kelly 1990 for a discussion of the two different modes of thermocapillary instability). The evolution equation provides an efficient alternative to the linear stability analysis of the full non-isothermal system, and enables us to study the weakly and fully nonlinear flow developments of the interface disturbance. For a precise control of a flat or corrugated interface, both the linear and the nonlinear flow behaviours need to be understood. We report the derivation of the evolution equation and the linear stability analysis here. The nonlinear evolution will be presented in a separate report.

2. Formulation

Two immiscible viscoelastic fluids are flowing in a vertical parallel-plate channel as shown in figure 1. The flow is induced by the combined effect of gravity and pressure gradient, so that the direction of the mean flow can be either vertically upward or downward in each phase. Each fluid has constant density ρ_i, thermal conductivity k_i and elastic time constants, where the index $i = 1$ ($i = 2$) represents fluid 1 (fluid 2), but the viscosity varies with local shear rate and temperature, as described below. The channel walls in contact with fluid 1 and 2 are maintained at constant temperatures T_1 and T_2, respectively.

We use a Cartesian coordinate system (x, y), measured in units of the channel gap d, where x is directed vertically downward and y is directed normal to plate 1 into the fluids. The non-dimensional time t, velocity $(u^{(i)}, v^{(i)})$, and stress components are based on the viscous scales of fluid 1, d^2/ν_1, ν_1/d, and $\rho_1\nu_1^2/d^2$, respectively, where $\nu_1 = \mu_{01}/\rho_1$ and μ_{01} is the zero-shear-rate viscosity of fluid 1 at temperature T_1. The

momentum equations for each phase are then written as

$$u_t^{(i)} + u^{(i)}u_x^{(i)} + v^{(i)}u_y^{(i)} = \frac{\rho_1}{\rho^{(i)}}\left[-p_x^{(i)} + \tau_x^{xx(i)} + \tau_y^{xy(i)}\right] + G, \tag{1}$$

$$v_t^{(i)} + u^{(i)}v_x^{(i)} + v^{(i)}v_y^{(i)} = \frac{\rho_1}{\rho^{(i)}}\left[-p_y^{(i)} + \tau_x^{xy(i)} + \tau_y^{yy(i)}\right], \tag{2}$$

where the subscripts x, y, and t represent partial differentiation. The components of the extra-stress tensor $\tilde{\tau}$ are denoted by superscripts for convenience. The parameter

$$G = \frac{d^3 g}{\nu_1^2}$$

is a measure of the gravity g. A parameter for the density ratio

$$\rho = \frac{\rho_2}{\rho_1}$$

appears in the momentum equations for fluid 2. The continuity equation for each phase is

$$u_x^{(i)} + v_y^{(i)} = 0. \tag{3}$$

For both fluids we modify the Oldroyd four-constant model to include the temperature dependency of the viscosity. The Oldroyd four-constant model describes viscoelasticity with shear thinning in dynamic viscosity and in first normal-stress coefficient but zero second normal-stress coefficient (see, e.g., Bird, Armstrong & Hassager (1987) for a detailed review of the model). We assume that the zero-shear-rate viscosity μ^{0i} varies linearly with temperature:

$$\mu^{0i} = \mu_{0i}\left[1 - \beta_i\left(\tilde{T} - T_1\right)\right], \tag{4}$$

where $\tilde{T}$ is the dimensional temperature. For most common fluids the constants β_i are positive (thermal thinning). If we scale the temperature using $T = (\tilde{T} - T_1)/(T_2 - T_1)$, the model becomes

$$\tilde{\tau}^{(i)} + De_{1i}\tilde{\tau}_*^{(i)} + \bar{Z}^{(i)}\left(\operatorname{tr}\tilde{\tau}^{(i)}\right)\tilde{\gamma} = \left(1 - \bar{B}^{(i)}T\right)(\tilde{\gamma} + De_{2i}\tilde{\gamma}_*), \tag{5}$$

where $\tilde{\gamma} = \nabla \boldsymbol{v} + (\nabla \boldsymbol{v})^T$ is the rate-of-strain tensor,

$$()_* = \frac{\mathrm{D}()}{\mathrm{D}t} - \left[() \cdot \nabla \boldsymbol{v} + (() \cdot \nabla \boldsymbol{v})^T\right], \tag{6}$$

superscript T denotes transpose, $\mathrm{D}/\mathrm{D}t$ is the material derivative, and $\nabla = (\partial_x, \partial_y)$ is the gradient operator. The parameters

$$De_{1i} = \frac{\nu_1 \lambda_{1i}}{d^2} \qquad \text{and} \qquad De_{2i} = \frac{\nu_1 \lambda_{2i}}{d^2}$$

are dimensionless relaxation and retardation time for each fluid, respectively, and become zero for inelastic fluids. For convenience we define the Deborah number in each phase as

$$De^{(i)} = De_{1i} - De_{2i},$$

which is always positive owing to the constraint of the model constants. The non-dimensional time constant

$$\bar{Z}^{(i)} = \frac{\nu_1 \eta_{0i}}{d^2}$$

and the parameter

$$\bar{B}^{(i)} = \beta_i (T_2 - T_1)$$

measure, respectively, the shear and the thermal thinning. For example, in a steady simple shear flow, the fluid viscosity would behave as

$$\mu_i = \mu^{0i} \frac{1 + \lambda_2 \eta_{0i} \dot{\gamma}^2}{1 + \lambda_1 \eta_{0i} \dot{\gamma}^2}. \tag{7}$$

The energy equations become, after non-dimensionalization,

$$\frac{\nu_1}{\nu_i} P^{(i)} \left(T_t^{(i)} + u^{(i)} T_x^{(i)} + v^{(i)} T_y^{(i)} \right) = T_{xx}^{(i)} + T_{yy}^{(i)}. \tag{8}$$

The Prandtl numbers

$$P^{(i)} = \frac{\nu_i}{\kappa_i},$$

where κ_i is the thermal diffusivity for each fluid. The kinematic-viscosity ratio

$$\nu = \frac{\nu_2}{\nu_1}$$

appears in the energy equation for fluid 2.

The interface between the fluids is located at $y = h(x,t)$, where $0 < h < 1$ due to the scaling. The mean location of the interface $h_0 = d_1/(d_1 + d_2)$ is imposed as a control parameter, where d_i is the mean layer thickness in each phase, but the local shape $h(x,t)$ must be obtained as a part of the solution to the above system. The interfacial tension σ varies linearly with temperature:

$$\sigma = \sigma_0 \left[1 - \gamma \left(\tilde{T} - T_1 \right) \right], \tag{9}$$

where σ_0 is the interfacial tension at $\tilde{T} = T_1$. There is a jump in the normal stress at the interface due to the capillary force:

$$-p^{(2)} + p^{(1)} + \left[\left[\boldsymbol{n} \cdot \tilde{\boldsymbol{\tau}}^{(i)} \cdot \boldsymbol{n} \right] \right] = -\frac{3}{N^3} \bar{S} h_{xx} \qquad \text{at} \quad y = h, \tag{10}$$

where

$$\boldsymbol{n} = \frac{1}{N} (-h_x, 1) \tag{11}$$

is the unit normal vector at the interface directed into fluid 2,

$$\bar{S} = \frac{\bar{\sigma}_0 d}{3 \rho_1 \nu_1^2}$$

is the non-dimensional mean interfacial tension, and $N = (1 + h_x^2)^{1/2}$. The jump in quantities across the interface is denoted by $[\![\cdot]\!] = (\cdot)^{(1)} - (\cdot)^{(2)}$. Owing to the thermocapillarity, there is a jump in the shear stress, which is described as

$$\left[\left[\boldsymbol{t} \cdot \tilde{\boldsymbol{\tau}}^{(i)} \cdot \boldsymbol{n} \right] \right] = M \boldsymbol{t} \cdot \nabla T \qquad \text{at} \quad y = h, \tag{12}$$

where

$$\boldsymbol{t} = \frac{1}{N} (1, h_x) \tag{13}$$

is the unit tangent vector at the interface. The Marangoni number, defined as

$$M = \frac{\gamma \sigma_0 d (T_2 - T_1)}{\rho_1 \nu_1^2},$$

measures the thermocapillarity, and can assume a positive or negative value depending on the controlled temperatures T_1 and T_2. There is no slip at the interface, so that

the normal and tangential components of the velocity vector are continuous across the interface:

$$[\![\boldsymbol{u}\cdot\boldsymbol{n}]\!] = 0 \qquad \text{at} \quad y = h, \tag{14}$$

$$[\![\boldsymbol{u}\cdot\boldsymbol{t}]\!] = 0 \qquad \text{at} \quad y = h. \tag{15}$$

The local temperature and heat flux are also continuous across the interface, which gives

$$T^{(1)} = T^{(2)} \qquad \text{at} \quad y = h \tag{16}$$

and

$$[\![k_i \boldsymbol{n}\cdot\nabla T^{(i)}]\!] = 0 \qquad \text{at} \quad y = h, \tag{17}$$

where the k_i are the thermal conductivities at each layer. The location of the interface is defined by the kinematic condition $v = h_t + uh_x$ at $y = h$, which is converted into

$$h_t + \left(\int_0^h u\,\mathrm{d}y\right)_x = 0 \tag{18}$$

by assuming the normal-velocity condition (14) and introducing a non-dimensional flow rate

$$Q = \int_0^1 u\,\mathrm{d}y,$$

which is in units of $v_1 d$. Here Q is positive (negative) for a vertically downward (upward) flow, and its magnitude can be considered as the Reynolds number. In the single-layer limit (μ_2, $\rho_2 \to 0$), it is impossible to impose the pressure gradient. The flow rate is controlled by changing the mean layer thickness, and the parameter G thus becomes the Reynolds number.

Both walls are rigid and kept at constant temperatures. The boundary conditions are thus

$$u^{(1)} = v^{(1)} = T^{(1)} = 0 \qquad \text{at} \quad y = 0, \tag{19}$$

$$u^{(2)} = v^{(2)} = 0 \quad \text{and} \quad T^{(2)} = 1 \qquad \text{at} \quad y = 1. \tag{20}$$

3. Evolution equation

When both layers are thin and the fluids have moderate elasticity (Q, G, $De^{(i)} = O(1)$), the instability occurs in the form of interfacial waves. The shear instability, which is essentially a short-wavelength disturbance of the Tollmien–Schlichting type, and the thermocapillary instability of the Pearson type (Pearson 1958), which also occurs for disturbance wavelength comparable to the layer thickness, do not exist. The interfacial modes start to grow for long-wave disturbances, while short waves are suppressed by the capillary force. The dynamics of the flow thus can be efficiently studied by applying the long-wave asymptotics. The interface deformation can have a profound effect on the quality of the processed materials, and needs to be thoroughly examined. While the linear stability of the interface can be studied by the usual infinitesimal-amplitude normal-mode analysis, as performed by Yih (1967) and Yiantsios & Higgins (1988) for isothermal Newtonian fluids and by Li (1969) and Su & Khomami (1992*a*) for isothermal viscoelastic fluids among others, we derive an evolution equation, which enables the stability analysis and the study of highly nonlinear flow behaviours beyond the initial disturbance growth. An equivalent

equation for isothermal Newtonian fluids has been reported by Tilley *et al.* (1994*a*), and the following is a rather tedious but straightforward extension of their derivation.

We apply the long-wave approximation by rescaling the streamwise and temporal variables to

$$\xi = \epsilon x \qquad \text{and} \qquad \tau = \epsilon t, \tag{21}$$

where the small parameter ϵ is the ratio of the channel gap d to a typical disturbance wavelength. The interfacial-tension parameter $\bar{S}$ is usually very large, but the shear and thermal thinning parameters, $\bar{Z}^{(i)}$ and $\bar{B}^{(i)}$, are small. We thus rescale these to

$$(\bar{S}, \bar{Z}^{(i)}, \bar{B}^{(i)}) = (\epsilon^{-2}S, \epsilon Z^{(i)}, \epsilon B^{(i)}) \tag{22}$$

while the other parameters are kept $O(1)$. The above scaling makes the leading-order solutions (basic state) purely Newtonian, and ensures that the stabilizing capillary force competes with the other destabilizing effects, appearing in the second order.

The dependent variables for each phase, including the stress components, are expanded for small ϵ:

$$u^{(i)} = u_0^{(i)} + \epsilon u_1^{(i)} + \cdots, \tag{23}$$

$$v^{(i)} = \epsilon \left(v_0^{(i)} + \epsilon v_1^{(i)} + \cdots \right), \tag{24}$$

$$p^{(i)} = \epsilon^{-1} \left(p_0^{(i)} + \epsilon p_1^{(i)} + \cdots \right), \tag{25}$$

$$\tau^{xx(i)} = \tau_0^{xx(i)} + \epsilon \tau_1^{xx(i)} + \cdots, \tag{26}$$

$$\tau^{xy(i)} = \tau_0^{xy(i)} + \epsilon \tau_1^{xy(i)} + \cdots, \tag{27}$$

$$\tau^{yy(i)} = \epsilon \left(\tau_0^{yy(i)} + \epsilon \tau_1^{yy(i)} + \cdots \right), \tag{28}$$

$$T^{(i)} = T_0^{(i)} + \epsilon T_1^{(i)} + \cdots. \tag{29}$$

The local layer thickness is taken to be of order unity. If we substitute these into the constitutive equation (5), we obtain the stress components as

$$\tau^{xx(i)} = 2\frac{\mu_{0i}}{\mu_{01}} De^{(i)} u_{0y}^{(i)2} + O(\epsilon), \tag{30}$$

$$\tau^{xy(i)} = \frac{\mu_{0i}}{\mu_{01}} \left[u_{0y}^{(i)} + \epsilon \left\{ u_{1y(i)} - De^{(i)} \left(\Phi_y^{(i)} - 2u_{0y}^{(i)} v_{0y}^{(i)} + 2Z^{(i)} u_{0y}^{(i)3} \right) - B^{(i)} u_{0y}^{(i)} T_0^{(i)} \right\} \right] + O(\epsilon^2), \tag{31}$$

$$\tau^{yy(i)} = \epsilon 2\frac{\mu_{0i}}{\mu_{01}} v_{0y}^{(i)} + O(\epsilon^2), \tag{32}$$

where

$$\Phi^{(i)} = u_{0\tau}^{(i)} + u_0^{(i)} u_{0\xi}^{(i)} + v_0^{(i)} u_{0y}^{(i)}. \tag{33}$$

The viscosity ratio

$$\mu = \frac{\mu_{02}}{\mu_{01}} = \rho v$$

appears for fluid 2.

In the leading order, we solve the y-momentum equations

$$p_{0y}^{(i)} = 0 \tag{34}$$

with

$$p_0^{(1)} = p_0^{(2)} \qquad \text{at} \quad y = h, \tag{35}$$

the x-momentum equations

$$0 = -p_{0\xi}^{(i)} + \frac{\mu_{0i}}{\mu_{01}} u_{0yy}^{(i)} + \frac{\rho_i}{\rho_1} G \tag{36}$$

with

$$u_0^{(1)} = 0 \qquad \text{at} \quad y = 0, \tag{37}$$

$$u_0^{(2)} = 0 \qquad \text{at} \quad y = 1, \tag{38}$$

$$u_0^{(1)} = u_0^{(2)} \qquad \text{at} \quad y = h, \tag{39}$$

$$u_{0y}^{(1)} = \mu u_{0y}^{(2)} \qquad \text{at} \quad y = h, \tag{40}$$

$$\int_0^h u_0^{(1)} \, \mathrm{d}y + \int_h^1 u_0^{(2)} \, \mathrm{d}y = Q, \tag{41}$$

the continuity equations

$$v_{0y}^{(i)} = -u_{0\xi}^{(i)} \tag{42}$$

with

$$v_0^{(1)} = 0 \qquad \text{at} \quad y = 0, \tag{43}$$

$$v_0^{(2)} = 0 \qquad \text{at} \quad y = 1, \tag{44}$$

and the energy equations

$$T_{0yy}^{(i)} = 0 \tag{45}$$

with

$$T_0^{(1)} = 0 \qquad \text{at} \quad y = 0, \tag{46}$$

$$T_0^{(2)} = 1 \qquad \text{at} \quad y = 1, \tag{47}$$

$$T_0^{(1)} = T_0^{(2)} \qquad \text{at} \quad y = h, \tag{48}$$

$$T_{0y}^{(1)} = k T_{0y}^{(2)} \qquad \text{at} \quad y = h, \tag{49}$$

where k $(= k_2/k_1)$ is a parameter measuring the thermal-conductivity ratio. As explained by Tilley *et al.* (1994*a*), five conditions are required for (36) because the leading-order pressure gradient $p_{0\xi}^{(1)}$ $(=p_{0\xi}^{(2)})$ has to be obtained simultaneously.

The solutions to the above system are

$$u_0^{(1)} = a_2^{(1)} y^2 + a_1^{(1)} y, \tag{50}$$

$$u_0^{(2)} = a_2^{(2)} (y-1)^2 + a_1^{(2)} (y-1), \tag{51}$$

$$T_0^{(1)} = \frac{ky}{1 + (k-1)h}, \tag{52}$$

$$T_0^{(2)} = \frac{y-1}{1 + (k-1)h}, \tag{53}$$

$$\vdots \tag{54}$$

where the coefficients $a_j^{(i)}(h; \rho, \mu, G, Q)$ are defined in the Appendix.

The second-order solutions are obtained in an identical sequence to that of the leading order, but we need to find only $p_{1\xi}^{(i)}$ and $u_1^{(i)}$ to obtain an evolution equation accurate to $O(\epsilon)$. Since all parameters introduced in the previous section are coupled in, the governing equations and solutions are very complicated. We have developed a

program in Macsyma that generates the complete solutions. The source code will be available to interested readers upon request. Here, we simply note that the capillary effect is introduced through the normal-stress interfacial condition

$$p^{(2)} - p^{(1)} = 3Sh_{\xi\xi} \qquad \text{at} \quad y = h \tag{55}$$

and the balance in viscous, elastic, thermal-thinning, and thermocapillary stressess is included in the shear-stress interfacial condition

$$\left[\left[-h_\xi \tau_0^{xx(i)} + \tau_1^{xy(i)}\right]\right] = M\left(T_{0\xi} + h_\xi T_{0y}\right) \qquad \text{at} \quad y = h. \tag{56}$$

Finally, the evolution equation can be obtained by substituting the solutions into the condition (18) (or the kinematic condition at the interface):

$$h_\tau + J_0 h_\xi + \epsilon\left(J_1 h_\xi + J_2 h_{\xi\xi\xi} + J_3\right)_\xi = 0, \tag{57}$$

where the coefficients

$$\begin{aligned} J_0 &= J_0(h; G, Q, \rho, \mu), \\ J_1 &= J_1\left(h; G, Q, \rho, \mu, k, De^{(i)}, M\right), \\ J_2 &= J_2(h; \mu, S), \\ J_3 &= J_3\left(h; G, Q, \rho, \mu, k, Z^{(i)}, B^{(i)}\right) \end{aligned}$$

are explained further in the following sections. The evolution equation for isothermal fluids is obtained by taking $M = B^{(i)} = 0$ in (57). If we further set $De^{(i)} = Z^{(i)} = 0$, the evolution equation for two Newtonian fluids, derived by Tilley *et al.* (1994*a*), is recovered except for the hydrostatic effect, which is absent in the present case of a vertical channel. The single-fluid limit is achieved by setting $\mu = \rho = 0$. If we take this limit with $M = B^{(i)} = 0$ on (57), the evolution equation for a vertical draining viscoelastic film, reported by Joo (1994), is obtained. If we then set $De^{(i)} = Z^{(i)} = 0$, the evolution equation for a Newtonian draining film, first obtained by Benney (1966), is recovered.

4. Interface-wave propagation

The terms proportional to J_0 and J_3 in (57) are considered as the convective terms, which govern the propagation of the disturbance downstream. Therefore, J_0 provides the nonlinear phase speed, while J_3 gives a small correction due to the shear and thermal thinning.

The leading-order phase speed J_0 is written as

$$J_0 = \frac{1}{f_0^2} h(h-1)E_0, \tag{58}$$

where

$$f_0(h; \mu) = h^4\mu^2 - 2h(h-1)(h^2 - h + 2)\mu + (h-1)^4 \tag{59}$$

is a positive-definite quantity and the factor $E_0 = E_0(h; G, Q, \rho, \mu)$. The local phase speed reduces to zero as the interface approaches either channel wall ($h \to 0$ or 1).

When there is no viscosity stratification ($\mu = 1$), the phase speed (58) becomes

$$J_0 = h(h-1)\left[Gh(2h-1)(h-1)(\rho - 1) - 6Q\right]. \tag{60}$$

It is seen that the phase speed increases linearly with the flow rate. Equation (60) also indicates that the local propagation speed of the interface disturbance

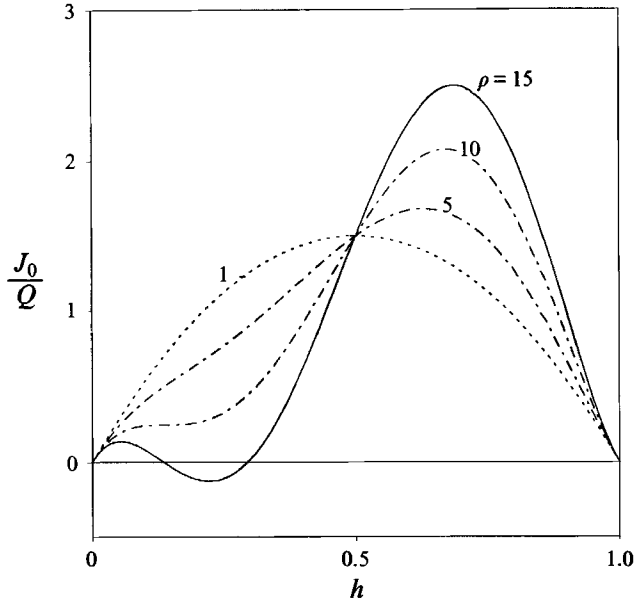

FIGURE 2. Local phase speed when $\mu = 1$ and $G = 5Q$.

decreases (increases) if the fluid with the higher density is locally thinner (thicker), i.e. $(2h-1)(\rho-1) < 0$. When $\rho = 1$, the phase speed reaches a maximum at the midpoint of the channel. When there is density difference between the fluids, the location is shifted toward the layer with higher density. This change in local phase speed is substantial when the density ratio ρ is very large. Figure 2 shows the phase speed J_0 against the interface location h for different values of ρ when $\mu = 1$, $G = 5$, and $Q = 1$. The interface location for the maximum phase speed moves closer to the wall 2 in contact with the higher-density fluid. Near the wall in contact with the lower-density fluid, the phase speed is lower. For sufficiently large density difference ($\rho = 15$), the minimum local phase speed can become negative, resulting in local wave propagation in the opposite direction to the flow.

In the absence of the density stratification ($\rho = 1$), we get

$$J_0 = \frac{6\mu}{f_0^2} h(h-1)\left(h^2\mu - h^2 + 1\right)\left(h^2\mu - 2h\mu - h^2 + 2h - 1\right) Q. \tag{61}$$

It is noteworthy that the local phase speed is now independent of G; it is proportional to the flow rate. At $\mu = (1-1/h)^2$ there is a reversal in the direction of the local wave propagation. If $\mu > (1-1/h)^2$, the wave propagates opposite to the flow direction.

If we assume that fluid 2 is inviscid ($\mu = 0$ but $\rho \neq 0$), a non-uniform limit

$$J_0 = Gh^2(1-\rho) \tag{62}$$

is obtained. It states that the disturbance does not propagate unless there is a density stratification and its direction, regardless of the location of the interface, depends on the density ratio. Equation (62) does not allow the interchange (for this case, switch ρ with $1/\rho$ and h with $1-h$) of fluid layers without changing the flow dynamics. This exchange must be performed before taking the non-uniform limit. If we further set $\mu = 0$ and $\rho = 0$, the expression

$$J_0 = Gh^2 \tag{63}$$

for a single fluid is obtained. When fluid 2 is absent, fluid 1 drains down owing to the gravity only, and we no longer have the freedom to impose the flow rate Q since the leading-order pressure gradient that drives Q vanishes in this limit: it is given as $Q = G/3$. The phase speed thus is proportional to G for a single fluid.

If the fluid viscosities change with local stress (shear thinning) or temperature (thermal thinning), there is a small correction

$$\epsilon \frac{\mathrm{d}J_3}{\mathrm{d}h}$$

to the phase speed J_0. For Newtonian fluids $J_3 = 0$, so that this phase shift is absent. The expression for J_3 can be divided into four parts:

$$\frac{\mathrm{d}J_3}{\mathrm{d}h} = J_{3Z} + J_{3B} = De^{(1)}Z^{(1)}J_{3Z}^{(1)} + De^{(2)}Z^{(2)}J_{3Z}^{(2)} + B^{(1)}J_{3B}^{(1)} + B^{(2)}J_{3B}^{(2)}, \tag{64}$$

where each part represents the contribution from shear and thermal thinning for each fluid layer and

$$J_{3Z}^{(i)} = J_{3Z}^{(i)}(h; G, Q, \rho, \mu), \tag{65}$$

$$J_{3B}^{(i)} = J_{3B}^{(i)}(h; G, Q, \rho, \mu, k). \tag{66}$$

The terms for shear thinning are linearly proportional to the Deborah number, and show that there is no shear-thinning contribution for inelastic fluids. From (64) it is interesting to note that each effect for each layer is combined as a simple linear superposition. This allows us to examine each term separately without losing the coupling of other competing effects†.

In the absence of density stratification, the shear-thinning effect is expressed by

$$J_{3Z} = \frac{1}{f_0^5} h(h-1)Q^3 \left(De^{(1)}Z^{(1)}E_{1Z}^{(1)} + De^{(2)}Z^{(2)}E_{1Z}^{(2)} \right), \tag{67}$$

where $E_{1Z}^{(i)} = E_{1Z}^{(i)}(h; \mu)$. It is very sensitive to the flow rate (proportional to Q^3), and disappears on either surface of the channel. When $\mu = 1$, only elastic stratification exists. In this case, we have

$$\frac{E_{1Z}^{(1)}}{f_0^5} = \frac{432}{5}\left(128h^5 - 320h^4 + 310h^3 - 150h^2 + 40h - 5\right), \tag{68}$$

$$\frac{E_{1Z}^{(2)}}{f_0^5} = -\frac{432}{5}\left(128h^5 - 320h^4 + 310h^3 - 140h^2 + 30h - 3\right). \tag{69}$$

These expressions have symmetry about $h = 1/2$ (h *vs.* $1 - h$), which correctly shows that the layers can be interchanged without affecting the phase speed if we also interchange $De^{(1)}$ with $De^{(2)}$. If we further set $De^{(1)} = De^{(2)}$ and $Z^{(1)} = Z^{(2)}$, we get

$$J_{3Z} = -\frac{864}{5} De^{(1)}Z^{(1)}Q^3 h(h-1)\left(5h^2 - 5h + 1\right), \tag{70}$$

which has two maxima at $h = 1/2 \pm \sqrt{3/20}$, a minimum at $h = 1/2$, and two zero points at $h = 1/2 \pm \sqrt{3/20}$. The shear thinning can either decrease or increase the phase speed. The shear-thinning effect for a single layer is seen by setting $\mu = \rho = 0$,

† This is also true for the full evolution equation (57), where each term again can be expressed as a linear superposition of further specified effects. The nonlinear coupling between all these effects is achieved through the interfacial motion $h(\xi, \tau)$.

which yields

$$J_{3Z} = 2De^{(1)}Z^{(1)}G^3h^4. \tag{71}$$

It is proportional to G^3 rather than Q^3 for the same reason as explained above. In contrast to stratified layers, the shear thinning always increases the phase speed.

The thermal-thinning effects are described by

$$J_{3B} = \frac{1}{f_0^3}h(h-1)Q\left(B^{(1)}E_{1B}^{(1)} + B^{(2)}E_{1B}^{(2)}\right), \tag{72}$$

for $\rho = 1$, where $E_{1B}^{(i)} = E_{1B}^{(i)}(h;\mu,k)$. They are linearly proportional to the flow rate, and disappear on the channel surface. If there is no stratification in density, viscosity, and thermal conductivety ($\rho = \mu = k = 1$), equation (72) is simplified to

$$\frac{E_{1B}^{(1)}}{f_0^3} = h(h-1)(6h^3 - 5h^2 + h), \tag{73}$$

$$\frac{E_{1B}^{(2)}}{f_0^3} = -h(h-1)(6h^3 - 5h^2 + h + 1). \tag{74}$$

These quantities are not symmetric about $h = 1/2$. Owing to the temperature gradient, interchanging the layers gives rise to different thermal-thinning effects. If we further set $B^{(1)} = B^{(2)}$, we get

$$J_{3Z} = -B^{(1)}Qh^2(h-1)^2. \tag{75}$$

When the interface is located closer to the channel wall with higher (lower) temperature, the phase speed increases (decreases) due to the thermal thinning. The single-layer limit ($\mu = \rho = 0$) for this case would represent stratified fluids, where fluid 2 is completely passive except for the conductive heat transfer from wall 2 to the interface. The thermal-thining effect

$$J_{3Z} = \frac{B^{(1)}Gkh^3}{3(hk - h + 1)} \tag{76}$$

always increases the phase speed.

The shear and thermal thinning do not affect the linear stability of the present flow system, as we shall see below. The nonlinear development of the unstable interface waves, however, will be greatly influenced by their effect on the local phase speed. For a single layer, the shear thinning is known to stabilize the interface motion and delay or suppress the chaotic flow development (Joo 1994). For stratified fluids, the shear- and thermal-thinning effects are not monotonic but a complicated function of the fluid properties and the interface location that varies with time. In order to study these effects further, we need to first identify the parametric regions where the interface wave may occur.

5. Stability analysis

The linear stability analysis of the stratified-flow system can be performed via the evolution equation. The basic state is a flat undisturbed interface, described by $h = h_0$, where h_0 is a constant. The velocity and temperature fields for this basic state can be obtained by substituting $h = h_0$ into the leading-order solutions described above. In both phases, the velocity distribution is parabolic and the heat transfer is purely conductive.

We superpose a simple harmonic disturbance of an infinitesimal amplitude onto the basic state, and write

$$h = h_0 + \delta \left(e^{i\alpha\xi + \Gamma\tau} + \text{c.c.}\right), \tag{77}$$

where α and Γ are the disturbance wavenumber and the complex growth rate, respectively, c.c. represents the complex conjugate, and $\delta \ll 1$. The linear stability of the system is then determined by the sense of the real part Γ_r of the growth rate; the disturbance will grow in time if $\Gamma_r > 0$. If we substitute (77) into the evolution equation and linearize in δ, we obtain

$$\Gamma_r = \epsilon\alpha^2 \left(J_1 - \alpha^2 J_2\right). \tag{78}$$

It is obvious that $J_1 > 0$ and $J_2 > 0$ will, respectively, destabilize and stabilize the flow.

The stabilizing term $\alpha^2 J_2$ has a factor α^2, so that it ensures the onset of instability to be at zero wavenumber and provides a cutoff wavenumber $\alpha_c = (J_1/J_2)^{1/2}$. The interfacial instabilities occur for disturbances with long wavelength because the capillary effect (J_2) suppresses short waves. The full expression for J_2 is given by

$$J_2 = -\frac{1}{f_0} h^3 (h-1)^3 (h\mu - h + 1) S, \tag{79}$$

which is positive definite for $0 < h < 1$ and $\mu > 0$; the capillary effect is always stabilizing. For convenience we will denote the basic state h_0 by h throughout the linear-stability analysis. As the viscosity ratio μ increases from zero, J_2 decays from the value for a single layer $h^3 S$ to zero. Since the the wavenumber α_M $(= (J_1/(2J_2))^{1/2}$ that corresponds to the maximum linear growth rate would increase to infinity as J_2 decays to zero, the long-wave asymptotics appears to break down for sufficiently large viscosity ratio μ. However, as we shall see below, the destabilizing effects in J_1 decay with the same rate as J_2 as μ increases to infinity, so that the evolution equation stays asymptotically valid for a large viscosity ratio.

While J_2 provides the wavenumber range for the instability, the other parametric regions for instability are obtained by studying J_1. Again, J_1 is given as a linear superposition of the effects of velocity-gradient jump at the interface (instability due to viscosity stratification), elastic normal stresses in both layers (elastic instability), and the surface-tension gradient (thermocapillary instability):

$$J_1 = J_{1V} + De^{(1)} J_{1E}^{(1)} + De^{(2)} J_{1E}^{(2)} + M J_{1T}, \tag{80}$$

where

$$J_{1V} = \frac{1}{f_0^5} h^2 (h-1)^2 E_{2V}(h; G, Q, \rho, \mu), \tag{81}$$

$$J_{1E}^{(i)} = \frac{1}{f_0} h^2 (h-1)^2 E_{2E}^{(i)}(h; G, Q, \rho, \mu), \tag{82}$$

$$J_{1T} = \frac{1}{f_0} h^2 (h-1)^2 E_{2V}(h; \mu, k). \tag{83}$$

5.1. *Instability due to density stratification*

As noted by Tilley *et al.* (1994*a*), the effect of density stratification is nonlinearly coupled in the evolution equation, and cannot be singled out as a linear superposition on other effects. If one wishes to examine the instability purely due to the density

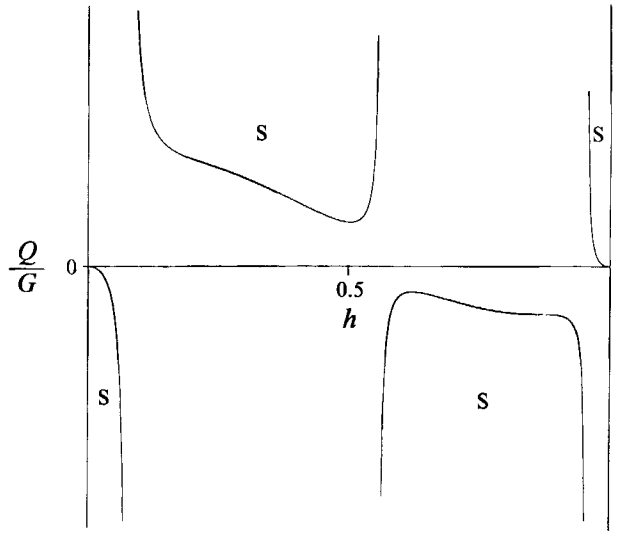

FIGURE 3. Instability due to the density stratification ($\rho > 1$). S denotes a stable region.

stratification, one can set $\mu = 1$ and $De^{(i)} = M = 0$ in (80) to obtain

$$J_1 = G(\rho - 1)h^3(h-1)^3 E_{2D}(h; Q, \rho). \tag{84}$$

The instability is of gravitational origin, and disappears as $G \to 0$.

When the layer thicknesses are equal ($h = 1/2$), J_1 is simplified to

$$J_1 = \frac{G}{1146880}(\rho - 1)^2 [(\rho + 1)G - 88Q], \tag{85}$$

which indicates that the flow becomes unstable if

$$Q < \frac{G}{88}(\rho + 1). \tag{86}$$

The flow rate must exceed a critical value to overcome the gravity-induced fluid redistribution. Flows opposing gravity ($Q < 0$) are always unstable.

If there is a thickness difference ($h \neq 1/2$), the effect of the density difference becomes more complicated. In figure 3, a stability diagram is shown for a density ratio $\rho > 1$, where the neutral stability curves are given by

$$\begin{aligned} Q/G = {} & \tfrac{1}{3}(\rho - 1)h^2(h-1)^2 \\ & \times(444h^5\rho - 1110h^4\rho + 1035h^3\rho - 479h^2\rho + 129h\rho - 19\rho - 444h^5 + 1110h^4 \\ & -1035h^3 + 406h^2 - 56h)/(384h^6\rho - 1152h^5\rho + 1295h^4\rho - 703h^3\rho + 211h^2\rho \\ & -37h\rho + 2\rho - 384h^6 + 1152h^5 - 1295h^4 + 637h^3 - 112h^2). \end{aligned} \tag{87}$$

As h increases or decreases from 1/2, the flow rate required to keep the flow stable increases. Further deviation from $h = 1/2$ eventually makes all vertically downward flows unconditionally unstable. As the thickness difference grows even further, the vertically downward flows become stable again for sufficiently large flow rate, if the thinner layer has higher fluid density. Similar conclusions can be drawn from the diagram for the destabilization of vertically upward flows. Since there is a symmetry

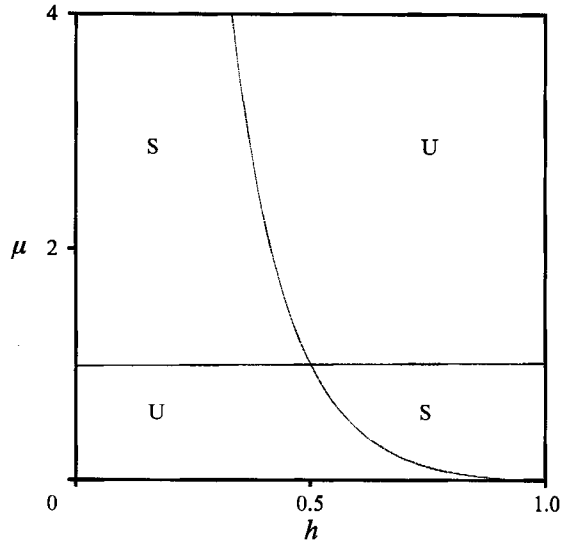

FIGURE 4. Instability due to the viscosity stratification. (As in Yiantsios & Higgins 1988.) S denotes stable and U unstable.

between ρ with h and $1/\rho$ with $1-h$, the stability diagram for $\rho < 1$ will be an exact mirror image of figure 3, and does not change the above stability criteria.

The density-stratification effect is coupled in the viscous and elastic instabilities, but does not affect the thermocapillary instabilities. In what follows, we will focus on these other instabilities by setting $\rho = 1$, except when we take the single-layer limit ($\mu = \rho = 0$).

5.2. *Instability due to viscosity stratification*

The linear-stability analysis for fluids with viscosity stratification has been reported extensively since the pioneering work by Yih (1967), and will not be repeated here. For completeness we will simply state some essential stability criteria, and expect the readers to refer to the more detailed studies by Yiansios & Higgins (1988) and, more recently, by Tilley *et al.* (1994*b*).

The term J_{1V} in (80) describes the instability due to the velocity-gradient difference at the interface, and can be written as

$$J_{1V} = Q^2 h^2 (h-1)^2 (\mu - 1)\left(h^2\mu - h^2 + 2h - 1\right) E_3(h;\mu), \tag{88}$$

where the density ratio is set to unity. The factor E_3 is positive definite for $\mu > 0$ and $0 < h < 1$, so that the flow becomes unstable if

$$(\mu - 1)\left[\mu - \left(\frac{1-h}{h}\right)^2\right] > 0. \tag{89}$$

Figure 4 illustrates this stability condition on a (μ, h)-plane. It shows that the instability occurs if the thinner layer is sufficiently more viscous. In layers with equal thickness ($h = 1/2$), the interface is always unstable.

If we take the single-layer limit $\mu = \rho = 0$ in (81), we recover the expression

$$J_1 = \frac{2}{15} G^2 h^6 \tag{90}$$

for the surface-wave instability. The flow becomes always unstable. The linear stability

and subsequent nonlinear flow developments for this case are explained in numerous works, including those by Yih (1963), Gjevik (1970), Lin & Wang (1985), Chang (1989), and Joo & Davis (1992*a*,*b*).

5.3. *Elastic instability*

When the fluid is viscoelastic, the extra normal stress, absent in purely viscous fluids, can cause the elastic instability. The two terms proportional to $De^{(1)}$ and $De^{(2)}$ in (80) model this elastic effect originating from fluids 1 and 2, respectively. In the absence of the density stratification, these are expressed by

$$J_{1E}^{(i)} = Q^2h^2\,(h-1)^2\left(h^2\mu - h^2 + 2h - 1\right)E_4^{(i)}(h;\mu). \tag{91}$$

The effect of viscosity stratification is coupled in these elastic effects, so that the term J_{1V} in (80) must be considered simultaneously, if one wishes to study the cases with $\mu \neq 1$.

Purely elastic instability can be studied by setting $\mu = 1$, which yields

$$J_1 = De^{(1)}J_{1E}^{(1)} + De^{(2)}J_{1E}^{(2)} = 36\left(De^{(2)} - De^{(1)}\right)Q^2h^2(h-1)^2(2h-1)^3. \tag{92}$$

The flow becomes unstable if the less (more) elastic fluid occupies more (less) than half of the channel,

$$\left(De^{(2)} - De^{(1)}\right)(2h-1) > 0, \tag{93}$$

a result reported by many others, including Su & Khomami (1992*b*) more recently. The elasticity thus can either stabilize or destabilize the interface, and its effect disappears when both layers are equally elastic or equal in thickness. It is interesting to note that the critical thickness $h = 1/2$ for stability/instability does not depend on the elasticity ratio, whereas in the viscous instability, described by (89), it varies with the viscosity ratio μ.

If we set $\mu = \rho = 0$, we recover the expression

$$J_{1E} = \tfrac{1}{3}G^2h^4 \tag{94}$$

for a single viscoelastic layer. It shows that the elasticity is always destabilizing in a draining film.

5.4. *Elastic instability with viscosity stratification*

The instabilities in viscoelastic layers with viscosity stratification are described by

$$\begin{aligned} J_1 &= J_{1V} + J_{1E}^{(1)} + J_{1E}^{(2)} \\ &= Q^2h^2\,(h-1)^2\left(h^2\mu - h^2 + 2h - 1\right)\left[(\mu-1)E_3 + De^{(1)}E_4^{(1)} + De^{(2)}E_4^{(2)}\right]. \end{aligned} \tag{95}$$

The growth rate has quadratic dependency on the flow rate, but the stability boundaries are not affected by the flow rate in layers with viscous and elastic instability.

When there is viscosity stratification ($\mu \neq 1$), the interface becomes unstable owing to both the velocity-gradient mismatch and the elasticity, even in the absence of elasticity stratification ($De^{(1)} = De^{(2)} = De$). Figure 5 shows the effect of fluid elasticity on the viscous instability, and vice versa. The viscosity ratio is taken to be $\mu = 2$. Since the fluids have no other distinction than viscosity and layer thickness, the behaviour for $\mu = 1/2$ can be easily deduced by symmetry. In figure 5(*a*), J_1/Q^2 is plotted against h for three different Deborah numbers, $De = 0$, 0.05, and 0.1. The horizontal axis can be considered as the neutral stability branch for all these Deborah numbers in the absence of viscosity stratification ($\mu = 1$). The curve for $De = 0$

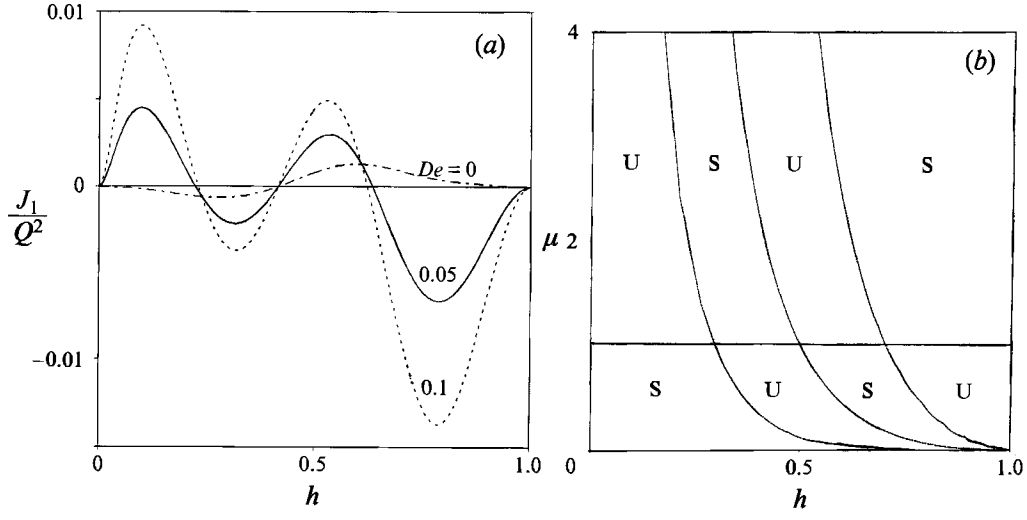

FIGURE 5. Instability due to the viscosity stratification and elasticity ($De^{(1)} = De^{(2)} = 0.1$). (*a*) Linear growth rate when $\mu = 2$; (*b*) stability diagram.

represents purely viscous instability. Since fluid 2 has twice the viscosity of fluid 1, the interface stays stable if $h < \sqrt{2} - 1$ and becomes unstable if $h > \sqrt{2} - 1$ (see (89)). When the fluids are viscoelastic ($De \neq 0$), each of these stable and unstable ranges is subdivided into another pair of stable and unstable ranges. When there is sufficient difference in layer thickness, the imbalance in the elastic normal stress will become large enough to change the stability boundary. If the more (less) viscous layer is thinner, it stabilizes (destabilizes) the flow. In fact, most dangerous modes (maximum growth rates) occur when $h \approx 0.1$, which lies in the stable range if the fluid were inelastic. In figure 5(*b*), the stability bounds are plotted in a (μ, h)-plane when $De = 0.1$. The branch that passes $(0.5, 1)$ is identical to that for purely viscous fluids in figure 4. The entire region to the right (left) of this branch would be unstable (stable) if $De = 0$. As the fluid elasticity increases from zero, a pair of new branches appears near $h = 0$ and $h = 1$, and approach each other. As seen in figure 5(*a*), for $\mu > 1$ these create an unstable region when the less-viscous layer is sufficiently thinner, and a stable region when it is sufficiently thicker. When $\mu < 1$, the opposite is true.

When there is elasticity stratification ($De^{(1)} \neq De^{(2)}$) as well, the elastic instability exists even in the absence of the viscosity stratification. Figure 6 shows the effect of the viscosity stratification on the elastic instability. In figure 6(*a*), fluid 2 has higher elasticity ($De^{(1)} = 0.1$ and $De^{(2)} = 0.2$). According to (93), the interface will become unstable if layer 2 is thinner ($h > 1/2$). However, for sufficiently large viscosity difference, additional stable and unstable regions appear, as explained in figure 5. A critical value for $\mu - 1$ (for $\mu > 1$) is required because the elasticity stratification further destabilizes (stabilizes) the viscous instability (stability). In the unstable and stable regions at the upper left and right corners, the effect of elasticity has overcome the effects of the stratifications in elasticity and viscosity. The stability criteria for $De^{(1)} > De^{(2)}$ can be deduced from figure 5(*a*) by considering the symmetry (h with μ and $1 - h$ with $1/\mu$). The resulting diagram is provided in figure 6(*b*) for reference.

5.5. *Thermocapillary instability*

Even when these is no elasticity and stratification in density and viscosity, the flow can become unstable due to the thermocapillarity. The full expression for this

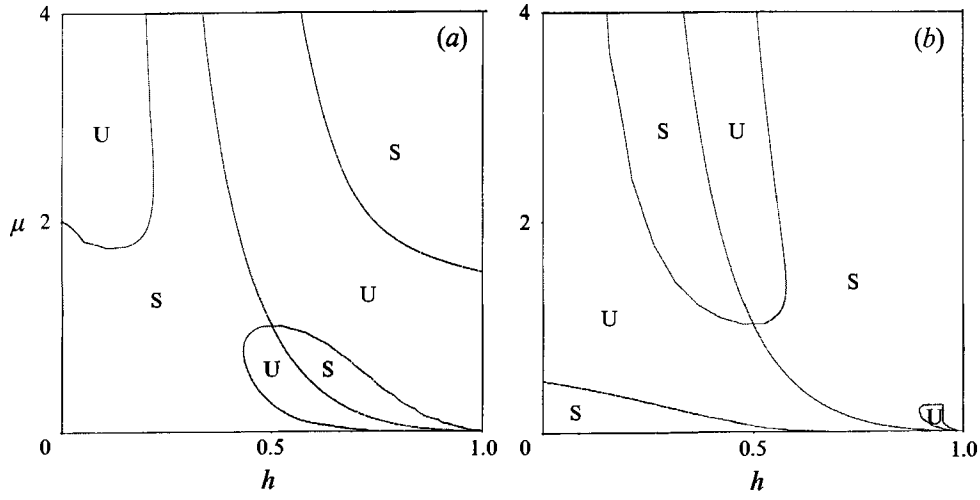

FIGURE 6. Instability due to the stratifications in viscosity and elasticity. (a) $De^{(1)} = 0.1$ and $De^{(2)} = 0.2$; (b) $De^{(1)} = 0.2$ and $De^{(2)} = 0.1$.

effect is

$$J_{1T} = -\frac{kh^2(h-1)^2\left(h^2\mu - h^2 + 2h - 1\right)}{2f_0\left[h(k-1)+1\right]^2}. \tag{96}$$

If we want to extract the purely thermocapillary instability, the viscosity ratio μ must be set to unity, which yields

$$J_{1T} = -\frac{h^2(h-1)^2(2h-1)k}{2\left[h(k-1)+1\right]^2}. \tag{97}$$

The interface will become unstable owing to the pure thermocapillarity if

$$M(2h-1) < 0 \tag{98}$$

or equivalently

$$(T_2 - T_1)(d_2 - d_1) > 0. \tag{99}$$

It can be deduced that the instability occurs if the channel wall in contact with the thicker layer is heated. If both layers are equal in thickness ($d_1 = d_2$), then the thermocapillarity becomes ineffective. The thermocapillarity also disappears in the limits either $k \to 0$ or $k \to \infty$.

5.6. *Thermocapillary instability with viscosity stratification*

When the viscosity stratification is also present, (96) must be considered with (88) superimposed:

$$J_1 = h^2(h-1)^2\left(h^2\mu - h^2 + 2h - 1\right)\left[Q^2(\mu-1)E_{3V} - M\frac{k}{2f_0\left[h(k-1)+1\right]^2}\right]. \tag{100}$$

The neutral stability branch related to (89) persists, but the flow can be stabilized or further destabilized, depending upon the heating condition M. The thermocapillarity is stabilizing if

$$M\left[\mu - \left(\frac{1-h_0}{h_0}\right)^2\right] < 0, \tag{101}$$

or equivalently,

$$(T_2 - T_1)\left(\frac{\mu_2}{\mu_1}d_1^2 - d_2^2\right) < 0. \tag{102}$$

Figure 7 shows the growth rate of the interface wave in layers with viscosity stratification and thermocapillarity. The viscosity ratio is set to $\mu = 2$, and several different values for M and k are chosen. The qualitative behaviour for $\mu = 1/2$ can be deduced from the figures owing to the symmetry. In figure 7(*a*), we set $k = 2$ and vary M from zero to 0.3. Since $k > 1$, the thermocapillarity by itself ($\mu = 1$) would stabilize the flow if $h > 1/2$ and destabilize if $h < 1/2$. The curve for $M = 0$ represents the purely viscous instability. The growth rate becomes positive if $h > \sqrt{2} - 1$, consistent with (89). The curve for $M = 0.1Q^2$ shows an unstable range of small h created by the thermocapillarity. The growth rate for $h > \sqrt{2} - 1$, on the other hand, has decreased. With a larger heating ($M = 0.2Q^2$), this effect is more conspicuous, and a stable range is created for large h. This trend continues for even larger heating, so that the new unstable region near $h = 0$ and the new stable region $h = 1$ expand toward each other until they collapse, resulting in complete reversal of stable and unstable ranges ($M = 0.3Q^2$). Figure 7(*b*) shows the growth rates for $k = 1/2$. In this case, the thermocapillarity destabilizes the flow for sufficiently large h. The two instabilities reinforce each other, and no change of stability criteria occurs. In figure 7(*c*), the same conditions as in figure 7(*a*) are taken except that a higher viscosity ratio ($\mu = 4$) is chosen. As the viscosity stratification increases, the thermocapillary destabilization near $h = 0$ becomes less effective. A small stable range of h near $h = 0$ survives the thermocapillarity if M is not sufficiently large ($M = 0.1Q^2$). This range would grow as the viscosity ratio μ grows.

In figure 8, the stability diagrams related to the cases in figure 7 (in particular, $k = 2$) are plotted on (μ, h)-planes. In all cases, the purely viscous branch that passes $(0.5, 1)$ is unaltered. Figure 8(*a*) shows the neutral stability curves for $M = 0.1Q^2$. If we follow a horizontal line $\mu = 2$, we recover the case $M = 0.1Q^2$ in figure 7(*a*). The branch $\mu = 1$ that exists in the purely viscous instability is here replaced by the curve that crosses the purely viscous branch that passes $(0.5, 1)$. There is a substantial increase in the unstable and stable regions that correspond to those for $\mu < 1$ in purely viscous instability (see figure 4). Therefore, even though the thinner layer is more viscous, the interface can stay stable, with appropriate heating or cooling of the channel walls. The new branch in the upper left corner is related to the M insufficient to change the viscous instability, discussed in figure 7(*c*). In figure 8(*b*), the heating is increased to $M = 0.2Q^2$. Both the destabilized and stabilized regions due to the thermocapillarity have expanded. Consequently, the stable region in the upper left corner has shrunk, and the peak near the upper right corner, which measures the penetration of the thermocapillary stabilization, has increased. The case $M = 0.2Q^2$ in figure 7(*a*) shows this stabilization effect for h near unity. If the thermocapillary effect is increased further, there is a complete stabilization (destabilization) of the unstable (stable) region of the purely viscous instability for viscosity ratios smaller than a critical value, as shown in figure 8(*c*). This critical value of μ increases with M. The instability due to viscosity stratification thus can be controlled by the thermocapillarity.

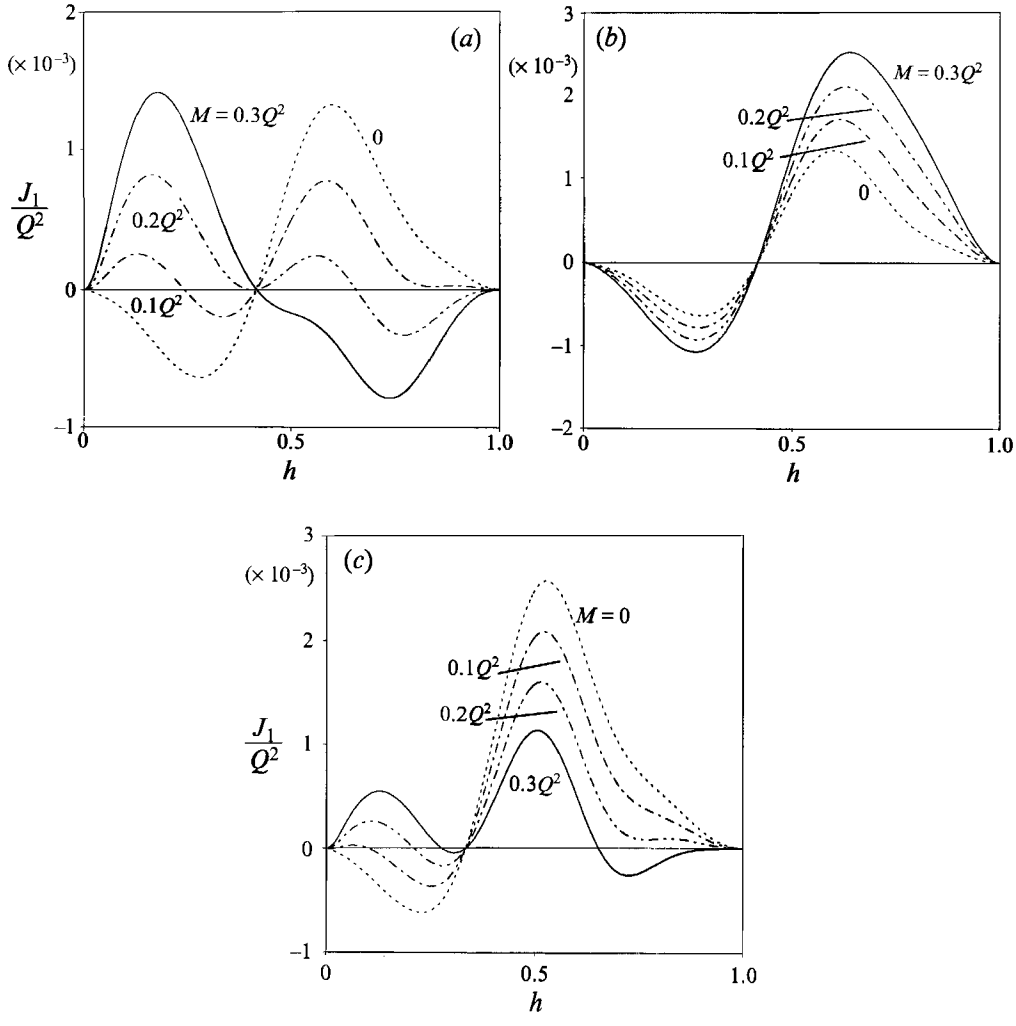

FIGURE 7. Linear growth rates in the presence of viscosity stratification and thermocapillarity. (*a*) $\mu = 2$ and $k = 2$; (*b*) $\mu = 2$ and $k = 1/2$; (*c*) $\mu = 4$ and $k = 2$.

5.7. *Thermocapillary instability with elasticity stratification*

The coupled instabilities due to the elasticity stratification and the thermocapillarity can be studied by superposing (93) with (97):

$$J_1 = h^2(h-1)^2(2h-1)\left[\left(De^{(2)} - De^{(1)}\right)Q^2(2h-1)^2 - M\frac{k}{2\left[h(k-1)+1\right]^2}\right]. \quad (103)$$

The elastic instability can be controlled by the thermocapillarity. Figure 9 provides the critical values of M for this stability control to be effective. The neutral branch for the purely elastic instability is the vertical line $h = 0.5$, to the right side of which the flow is elastically unstable. A few thermocapillary branches are plotted in the diagram, each corresponding to different values of the thermal conductivity ratio k. If $k = 1$ the thermocapillarity is inactive, so that the branch coincides with $h = 0.5$. As k deviates from unity, the thermocapillary branch widens, resulting in the expansion of new stable and unstable regions due to the thermocapillarity. From the first (second)

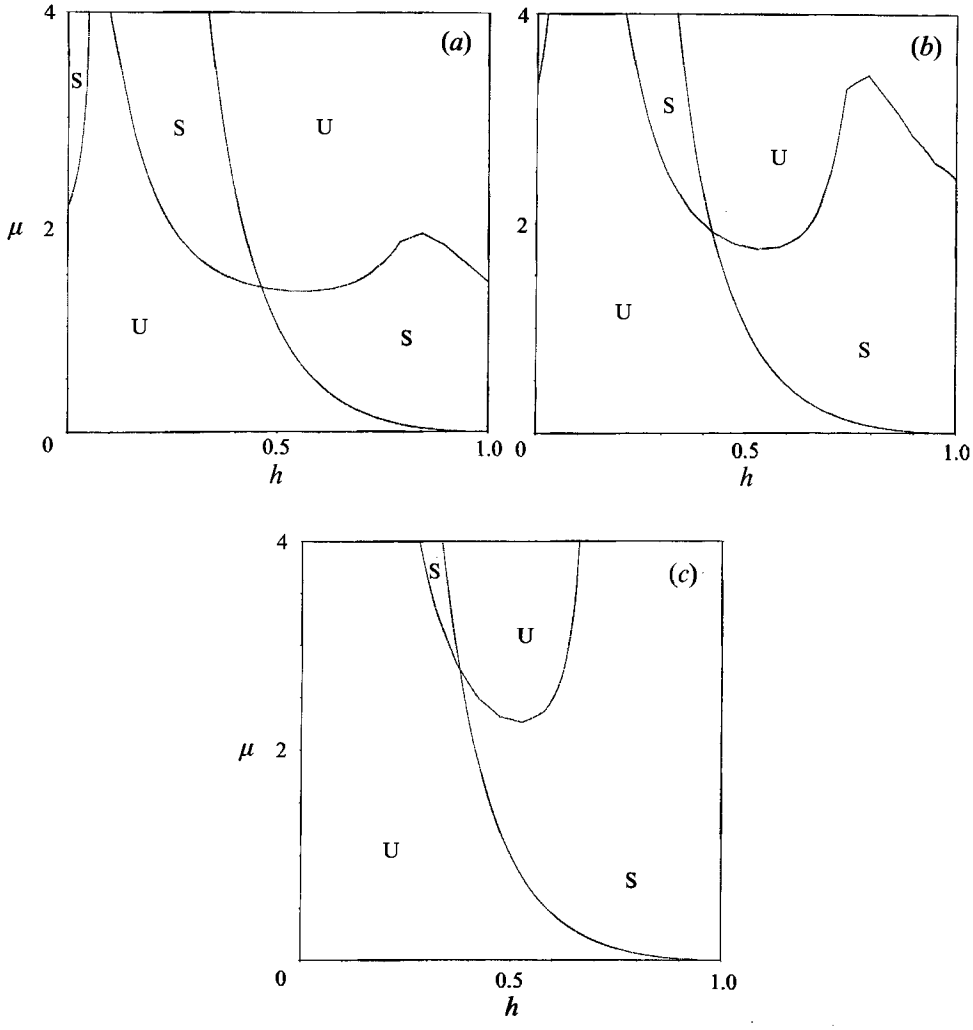

FIGURE 8. Instability due to viscosity stratification and thermocapillarity when $k = 2$. (*a*) $M = 0.1Q^2$; (*b*) $M = 0.2Q^2$; (*c*) $M = 0.3Q^2$.

quadrant of the diagram we can deduce that if the fluid in contact with the heated wall has the higher thermal conductivity and elasticity and smaller (larger) thickness, the thermocapillarity stabilizes (destabilizes) the interface. The amount of heating required decreases with the increase of k. As $k \to \infty$ the thermocapillary term in the above equation behaves as $M/(2h^2)$, so that a complete destabilization will occur near $h = 0$, whereas a complete stabilization will not occur near $h = 1$. If the fluid in contact with the temperature-controlled side has smaller thermal conductivity (third and fourth quadrant), $M/\left(De^{(2)} - De^{(1)}\right)$ has to be negative for the thermocapillary stablization and destabilization to occur. Therefore, the fluid with the lower elasticity must be in contact with the wall with the higher temperature.

5.8. *Thermocapillary instability with viscosity stratification and elasticity*

In order to examine the effect of thermocapillarity on viscoelastic fluids with viscosity stratification, the full equation (80) should be considered. In the absence of density stratification, each term has a common factor $(h^2\mu - h^2 + 2h - 1)$, which corresponds

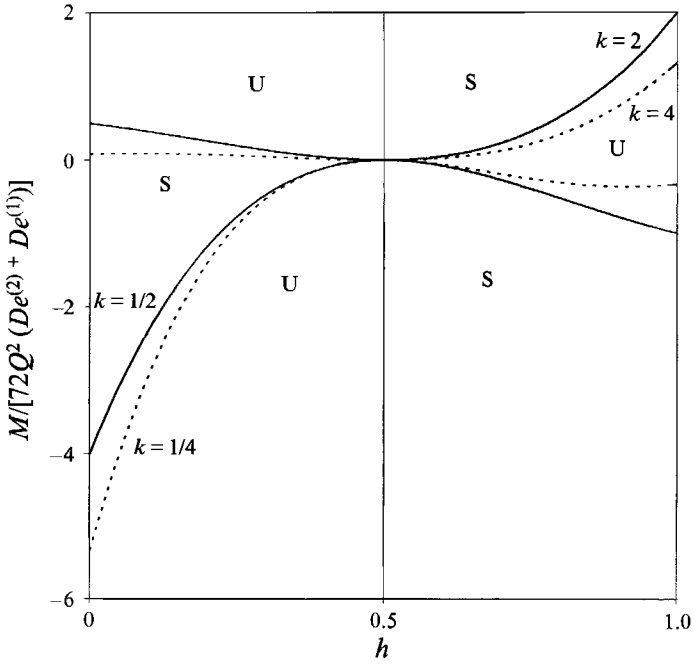

FIGURE 9. Instability due to elasticity and thermocapillarity when $\mu = 1$.

to the neutral branch of the purely viscous instability. This branch thus is not affected by elasticity or thermocapillarity. Other branches, on the other hand, are influenced by the interaction of elasticity, stratification of elasticity, and thermocapillarity.

Figure 10 shows stability diagrams in (μ, h)-planes when there is no elasticity stratification ($De^{(1)} = De^{(2)} = 0.1$), wall 2 is heated ($M > 0$), and fluid 2 has higher thermal conductivity ($k = 2$). Except for the thermocapillarity, the cases are identical to that in figure 5(b). In figure 10(a), we set $M = 0.1Q^2$. Since $M(k - 1) > 0$, the thermocapillarity by itself is stabilizing if $h > 1/2$ and destabilizing if $h < 1/2$. Consequently, compared to the isothermal case in figure 5(b), the stable (unstable) region to the right (left) of the viscous neutral branch has expanded. The branch $\mu = 1$ that exists in the isothermal case has disappeared. If we enhance the thermocapillary effect, the expansion of these stable and unstable regions develop further, as shown in figure 10(b) for $M = Q^2$.

In figure 11, the stability diagrams are shown for cases where the elasticity stratification ($De^{(1)} \neq De^{(2)}$) is also present and $M = Q^2$. In figure 11(a), the fluid in the heated side is more elastic ($De^{(1)} = 0.1Q^2$ and $De^{(2)} = 0.2Q^2$). The isothermal counterpart is shown in figure 6(a). Two unstable regions to the left of the viscous neutral branch have merged together, and a new unstable region has been created at the lower left corner of the diagram. The opposite case of the elasticity stratification ($De^{(1)} = 0.2Q^2$ and $De^{(2)} = 0.1Q^2$) is shown in figure 11(b). Compared to the isothermal case in figure 6(b), the stable region in the lower left corner has completely disappeared, whereas the unstable region in the lower right corner persists. The viscosity ratio μ for the instability to set in to the right of the viscous neutral branch has been increased.

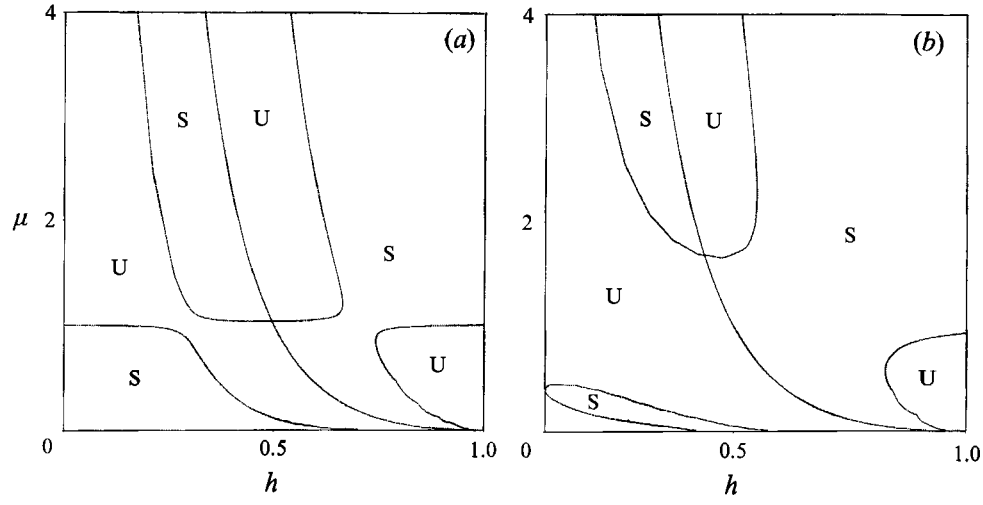

FIGURE 10. Instability due to elasticity and thermocapillarity when $k = 2$ and $De^{(1)} = De^{(2)} = 0.1$. (*a*) $M = 0.1Q^2$; (*b*) $M = Q^2$.

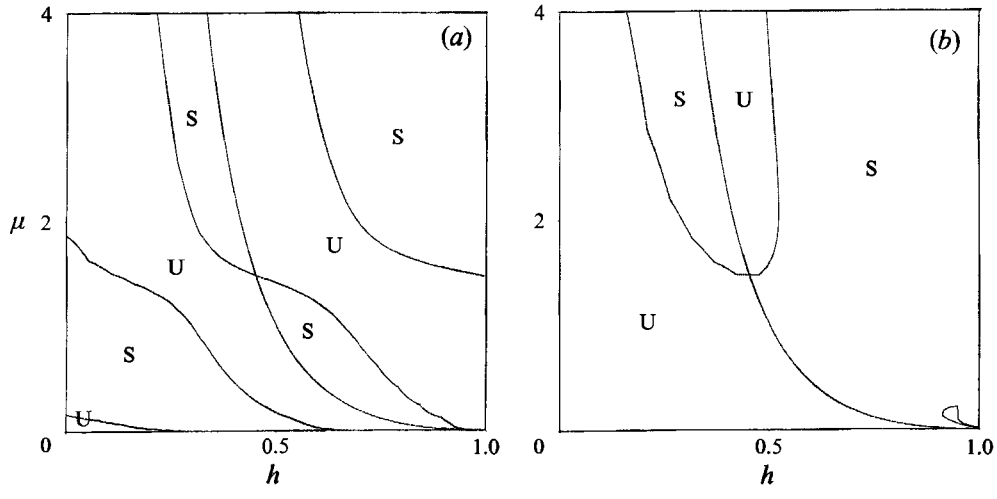

FIGURE 11. Instability due to thermocapillarity and stratifications in viscosity and elasticity when $k = 1$ and $M = Q^2$. (*a*) $De^{(1)} = 0.1$ and $De^{(2)} = 0.1$; (*b*) $De^{(1)} = 0.1$ and $De^{(2)} = 0.1$.

6. Concluding remarks

An evolution equation is derived that predicts the motion of the interface between two thin viscoelastic fluids with shear thining, thermal thinning, and thermocapillarity. For thin layers, the present approach provides reasonable grounds for studying the linear stability and subsequent nonlinear flow developments of the interface encountered in many engineering applications. The equation models the effects of shear and thermal thinning, which modify the propagation of the interface waves, and elasticity, thermocapillarity, and the stratification of fluid density, viscosity, and elasticity, which affect the stability of the interface.

The linear stability analysis performed via the evolution equation reveals the competing effects of viscosity stratification, elasticity, and thermocapillarity. The instability due to the viscosity stratification that exists whenever the more viscous layer is suf-

ficiently thinner and the instability due to the elasticity or the elasticity stratification can be controlled by the thermocapillarity. The stability analysis presented in this study can be used to determine the appropriate temperatures to be imposed on the channel walls. All the fluid properties introduced in the analysis, the imposed flow rate, and the desired thickness ratio affect these conditions.

While the linear-stability analysis is useful in obtaining the global picture of the flow conditions for stability or instability, it is important to understand the nonlinear developments of the interface waves beyond the initial linear instability. The evolution equation renders an efficient alternative to the direct numerical simulation of the full coupled system. A dynamical-system analysis and spectral computations are performed through the evolution equation, and the results will be reported in Part 2 of the study.

Appendix.

The coefficients for the leading-order velocity profiles, (50)–(51), are given as follows.

$$a_1^{(1)} : \{((gh^5 - 4gh^4 + 5gh^3 - 2gh^2)\mu - gh^5 + 4gh^4 - 6gh^3 + 4gh^2 - gh)\rho + (6h^2\mu^2 + (-6h^2 + 6)\mu)qq + (-gh^5 + 4gh^4 - 5gh^3 + 2gh^2)\mu + gh^5 - 4gh^4 + 6gh^3 - 4gh^2 + gh\}/\{h^4\mu^2 + (-2h^4 + 4h^3 - 6h^2 + 4h)\mu + h^4 - 4h^3 + 6h^2 - 4h + 1\}.$$

$$a_2^{(1)} : \{((gh^4 - 6gh^3 + 9gh^2 - 4gh)\mu - gh^4 + 4gh^3 - 6gh^2 + 4gh - g)\rho + (12h\mu^2 + (-12h + 12)\mu)qq + (-gh^4 + 6gh^3 - 9gh^2 + 4gh)\mu + gh^4 - 4gh^3 + 6gh^2 - 4gh + g\}/\{2h^4\mu^2 + (-4h^4 + 8h^3 - 12h^2 + 8h)\mu + 2h^4 - 8h^3 + 12h^2 - 8h + 2\}.$$

$$a_1^{(2)} : \{((gh^5 - gh^4)\mu - gh^5 + gh^4 + gh^3 - gh^2)\rho + ((6h^2 - 12h)\mu - 6h^2 + 12h - 6)qq + (-gh^5 + gh^4)\mu + gh^5 - gh^4 - gh^3 + gh^2\}/\{h^4\mu^2 + (-2h^4 + 4h^3 - 6h^2 + 4h)\mu + h^4 - 4h^3 + 6h^2 - 4h + 1\}.$$

$$a_2^{(2)} : -\{(gh^4\mu - gh^4 - 2gh^3 + 3gh^2)\rho + (12h\mu - 12h + 12)qq - gh^4\mu + gh^4 + 2gh^3 - 3gh^2\}/\{2h^4\mu^2 + (-4h^4 + 8h^3 - 12h^2 + 8h)\mu + 2h^4 - 8h^3 + 12h^2 - 8h + 2\}.$$

REFERENCES

BENNEY, D. J. 1966 Long waves in liquid films. *J. Math. Phys.* **45**, 150–155.

BIRD, R. B., ARMSTRONG, R. C. & HASSAGER, O. 1987 *Dynamics of Polymeric Liquids*, Vol. 1, Chapter 7. Wiley-Interscience.

CHANG, H.-C. 1989 Onset of nonlinear waves on falling films. *Phys. Fluids* A **1**, 1314–1327.

CHARRU, F. & FABRE J. 1994 Long waves at the interface between two viscous fluids. *Phys. Fluids* **6**, 1223–1235.

CHEN, K.-P. 1991 Interfacial instability due to elastic stratification in concentric coextrusion of two viscoelastic fluids. *J. Non-Newtonian Fluid Mech.* **40**, 155–175.

GJEVIK, B. 1970 Occurence of finite-amplitude surface waves on falling liquid films. *Phys. Fluids* **13**, 1918–1925.

GOUSSIS, D. A. & KELLY, R. W. 1990 On the thermocapillary instabilities in a liquid layer heated from below. *Intl J. Heat Mass Transfer* **33**, 2237–2245.

HOOPER, A. P. & GRIMSHAW, R. 1985 Nonlinear instability at the interface between two viscous fluids. *Phys. Fluids* **28**, 37–45.

JOO, S. W. 1994 The stability and nonlinear flow developments of a viscoelastic draining film with shear thinning. *J. Non-Newtonian Fluid Mech.*, **51**, 125–140.

JOO, S. W. & DAVIS, S. H. 1992*a* Instabilities of three-dimensional viscous falling films. *J. Fluid Mech.* **242**, 529–547.

JOO, S. W. & DAVIS, S. H. 1992*b* Irregular waves on viscous falling films. *Chem. Engng Commun.* **118**, 111–123.

LARSON, R. G. 1992 Instabilities in viscoelastic fluids. *Rheol. Acta* **31**, 213–239.

LI, C.-H. 1969 Stability of two superposed elasticoviscous liquids in plane Couette flow. *Phys. Fluids* **12**, 531–538.

LIN, S.-P. & WANG, C.-Y. 1985 *Encyclopedia of Fluid Mechanics*, vol. 1, p. 931. Gulf.

NORDBERG, M. E. & WINTER, H. H. 1990 A simple model of nonisothermal coextrusion. *Polymer Engng Sci.* **30**, 408–415.

PEARSON, J. R. A. 1958 On convection cells induced by surface tension. *J. Fluid Mech.* **4**, 489–500.

RENARDY, M. & RENARDY, Y. 1993 Derivation of amplitude equations and analysis of sideband instabilities in two-layer flows. *Phys. Fluids* A **5**, 2738–2762.

RENARDY, Y. 1988 Stability of the interface in two-layer Couette flow of upper convected Maxwell liquids. *J. Non-Newtonian Fluid Mech.* **28**, 99–115.

SORNBERGER, G., VERGNES, B. & AGASSANT, J. F. 1986 Coextrusion flow of two molten polymers between parallel plates: non- isothermal computation and experimental study. *Polymer Engng Sci.* **26**, 682–689.

SU, Y.-Y. & KHOMAMI, B. 1992*a* Interfacial stability of multilayer viscoelastic fluids in slit and converging channel die geometries. *J. Rheol.* **36**, 357.

SU, Y.-Y. & KHOMAMI, B. 1992*b* Pure elastic interfacial instabilities in superposed flow of polymeric fluids. *Rheol. Acta* **31**, 413–420.

TILLEY, B. S., DAVIS, S. H. & BANKOFF, S. G. 1994*a* Nonlinear long-wave stability of superposed fluids in an inclined channel. *J. Fluid Mech.* **277**, 55–83.

TILLEY, B. S., DAVIS, S. H. & BANKOFF, S. G. 1994*b* Linear stability theory of two-layer flow in an inclined channel. *Phys. Fluids* **6**, 3906–3922.

YIANTSIOS, S. G. & HIGGINS, B. G. 1988 Linear stability of plane Poiseuille flow of two superposed fluids. *Phys. Fluids* **31**, 3225–3238.

YIH, C.-S. 1963 Stability of liquid flow down an inclined plane. *Phys. Fluids* **6**, 321–334.

YIH, C.-S. 1967 Instability due to viscosity stratification. *J. Fluid Mech.* **27**, 337–352.